Mon. Not. R. Astron. Soc. **422,** 2661–2674 (2012) doi:10.1111/j.1365-2966.2012.20836.x

Fast X-ray transients towards the Galactic bulge with the *Rossi X-ray Timing Explorer*

D. M. Smith,[1,2]★ C. B. Markwardt,[3] J. H. Swank[3] and I. Negueruela[4]

[1]*Physics Department and Santa Cruz Institute for Particle Physics, University of California, Santa Cruz, 1156 High Street, Santa Cruz, CA 95064, USA*
[2]*Space Sciences Laboratory, University of California, Berkeley, CA, USA*
[3]*NASA's Goddard Space Flight Centre, Greenbelt, MD, USA*
[4]*Departamento de Física, Ingeniería de Sistemas y Teoría de la Señal, Universidad de Alicante, Alicante, Spain*

Accepted 2012 February 27. Received 2012 February 27; in original form 2011 December 8

ABSTRACT

In X-ray binaries, rapid variability in X-ray flux of greater than an order of magnitude on timescales of a day or less appears to be a signature of wind accretion from a supergiant companion. When the variability takes the form of rare, brief, bright outbursts with only faint emission between them, the systems are called supergiant fast X-ray transients (SFXTs). We present data from twice-weekly scans of the Galactic bulge by the *Rossi X-ray Timing Explorer* that allow us to compare the behaviour of known SFXTs and possible SFXT candidates with the persistently bright supergiant X-ray binary 4U 1700−377. We independently confirm the orbital periods reported by other groups for SFXTs SAX J1818.6−1703 and IGR J17544−2619. The new data do not independently reproduce the orbital period reported for XTE J1739−302, but slightly improve the significance of the original result when the data are combined. The bulge source XTE J1743−363 shows a combination of fast variability and a long-term decline in activity, the latter behaviour not being characteristic of supergiant X-ray binaries. A far-red spectrum of the companion suggests that it is a symbiotic neutron star binary rather than a high-mass binary, and the reddest known of this class: the spectral type is approximately M8 III.

Key words: accretion, accretion discs – binaries: symbiotic – stars: neutron – supergiants – X-rays: binaries.

1 INTRODUCTION

Blue supergiant stars were first identified with fast X-ray transients discovered by *ASCA* (AX 1845.0−0433; Yamauchi et al. 1995; Coe et al. 1996) and later by *Rossi X-ray Timing Explorer (RXTE)* (XTE J1739−302; Smith et al. 1998; Smith 2003). As more began to be discovered with *INTEGRAL*, they were recognized as a class (Smith 2004; in't Zand 2005; Sguera et al. 2005; Negueruela et al. 2006) and named supergiant fast X-ray transients (SFXTs; Negueruela et al. 2006).

SFXTs are thought to be a subclass of X-ray binary in which a neutron star accretes the wind of a supergiant companion. Some binaries with these two components have been known since the 1970s as very bright and variable X-ray sources (e.g. Vela X-1, 4U 1700−377), but the SFXTs spend most of their time at low luminosities of 10^{32} to 10^{34} erg s^{-1}, with only very brief excursions to outburst luminosities of up to a few times 10^{36} erg s^{-1}. These outbursts generally last for several hours, with subpeaks lasting for minutes (e.g. Rampy, Smith & Negueruela 2009; Sidoli et al. 2009).

The cause of this behaviour is not known. Clumps in the wind of the companion can explain rapid variability within outbursts (in't Zand 2005; Walter & Zurita Heras 2007; Negueruela et al. 2008a), but are less successful at explaining long periods of quiescence. In some cases a highly eccentric or wide orbit may be responsible (Sidoli et al. 2007), but some SFXTs have been shown to have orbits as short as the persistently bright sources (see Table 1). Rejection of the wind material by the magnetic propeller effect (Grebenev & Sunyaev 2007; Bozzo, Falanga & Stella 2008a; Li & Zhang 2011) has been suggested. Depending on the particular systems studied and the assumptions made about the accretion physics, consideration of the propeller effect has led to both high lower limits ($>10^{13}$ G; Bozzo et al. 2008a) and low upper limits ($>10^{10}$ G; Li & Zhang 2011) on the magnetic field. Unexpected structure in the companion wind itself, e.g. very rare clumps with a very high density contrast, has not yet been ruled out.

Some sources have been referred to as intermediate between SFXTs and the familiar persistent supergiant/neutron star binaries, but this category has never been universally defined. The most common criterion for 'intermediateness' mentioned in the literature is the dynamic range between the highest and lowest luminosities observed. 'Intermediate' sources by this criterion have been defined

★E-mail: dsmith8@ucsc.edu

Table 1. System characteristics for eight fast transients.

Name	Companion	Distance	Period
XTE J1739−302	O8Iab(f) (1,2)	2.7 (2)	51.47 ± 0.02 (3)
IGR J17544−2619	O9Ib (4)	3.6 (2,4)	4.926 ± 0.001 (5)
4U 1700−377	O6.5Iaf+ (6)	1.9, 2.1 (6,7)	3.411 61 ± 0.000 05 (8)
SAX J1818.6−1703	∼B0I (9,10)	2, 2.1 (10,11)	30.0 ± 0.2 (12,13)
AX J1845.0−0433	O9Ia (14)	7 (14)	Unknown
IGR J16479−4514	O8.5I, O9.5Iab (2,15)	4.9, 2.8 (2,15)	3.3194 ± 0.001 (16,17)
XTE J1743−363	Unknown	Unknown	Unknown
XTE J1901+014	Faint in *K* (10)	1–7 kpc (10,18)	Unknown

(1) Negueruela et al. (2006); (2) Rahoui et al. (2008); (3) Drave et al. (2010); (4) Pellizza, Chaty & Negueruela (2006); (5) Clark et al. (2009); (6) Ankay et al. (2001); (7) Megier et al. (2009); (8) Hong & Hailey (2004); (9) Negueruela & Schurch (2007); (10) Torrejón et al. (2010); (11) Negueruela, Torrejón & Reig (2008); (12) Zurita Heras & Chaty (2009); (13) Bird et al. (2009); (14) Negueruela et al. (2007); (15) Nespoli, Febregat & Mennickent (2008); (16) Jain, Paul & Dutta (2009); (17) Romano et al. (2009); (18) Karasev, Lutovinov & Burenin (2008).

as either those with a dynamic range of <100 but >20 or so (Walter & Zurita Heras 2007; Clark et al. 2010) or those with a range of 100–1000 (Sguera et al. 2011; Romano et al. 2012). The maximum dynamic range of any source – both the SFXTs and the classical wind-accreting high mass X-ray binaries (HMXBs) such as Vel X-1 – can only increase with the number of observations made. Thus it is not surprising that the most recent of these references give the higher range for intermediate systems, since the known dynamic ranges of all the objects have increased in recent years. Chaty (2010) adds two additional criteria to the definition of intermediateness: a higher average luminosity than the canonical SFXTs and a longer average duration for individual flares. Romano et al. (2012) add the criterion that the lowest luminosity frequently observed should be close to 10^{35} erg s^{-1} for intermediate systems, and one to two orders of magnitude lower for true SFXTs. Romano et al. (2011) have begun to make the SFXT versus intermediate classification systematic for the first time by interpreting histograms of the luminosity of three sources, XTE J1739−302, IGR J17544−2619 and IGR J16479−4514, made from monitoring data from the sensitive *Swift* X-ray Telescope (XRT). The difference between true SFXT and intermediate systems in that work is based on the fraction of time spent at the lowest luminosities.

2 DATA AND ANALYSIS

We present data from the Galactic bulge scan programme (Swank et al. 2001) of the Proportional Counter Array (PCA) instrument on *RXTE* (Jahoda et al. 2006). PCA is a large-area X-ray detector with a collimated but non-imaging field of view of 1° full width at half-maximum. Twice a week, PCA scans the inner Galaxy in a raster pattern, recording the instantaneous 2–10 keV count rate of a large catalogue of sources. The bulge scan data are publicly available.[1]

In this paper we show data from the two 'prototype' SFXTs XTE J1739−302 and IGR J17544−2619 (Figs 1 and 2), the persistently bright wind accretor 4U 1700−377 (Fig. 3), three supergiant binaries that are not well studied and have been considered either SFXTs or 'intermediate' systems (SAX J1818.6−1703, AX J1845.0−0433 and IGR J16479−4514; Figs 4, 5 and 6, respectively), and finally two fast transients whose companion type and nature are not known: XTE J1743−363 and XTE J1901+014 (Figs 7 and 8). For each source we present four complementary views of the data: the 2–10 keV light curve from up to 12 years of bulge scans, a Lomb-normalized periodogram used to search for orbital periodicity, an integral histogram of the luminosities and the autocorrelation function of the light curve.

The light curves can be considered reliable at relatively high count rates, but near zero counts the results are complicated by the systematic limitations of the technique of fitting the count rate time profiles of the raster scans. For example, systematic uncertainties in the profile of the Galactic 'diffuse' emission (much of which may be an ensemble of many faint cataclysmic variables and other stars – see Revnivtsev et al. 2006) translate to uncertainties in the lowest source count rate. This problem is particularly severe for AX J1845.0−0433 (Fig. 5a), where the bifurcated appearance of the baseline values is caused by the alternation of scans parallel and perpendicular to the Galactic plane. The very large error bars for IGR J16479−4514 (Fig. 6a) are due to the proximity of the bright low-mass X-ray binary GX 340+0. We therefore cannot draw conclusions about the fluxes of the latter two objects outside of outburst. The counts shown are normalized to be the expected 2–10 keV count rate if all five detectors making up the PCA were turned on. In practice, one to five detectors are on at any given time, and this will be reflected in varying error bars from point to point. In these units, the Crab would be of the order of 10 000 counts s^{-1}.

The second panels (b) of Figs 1–8 show the Lomb-normalized periodogram of the data, used to search for orbital periods. The grey horizontal line represents the largest expected value for each period in 10^4 randomized trials (the real data values were randomly reassigned to the real data acquisition times in each trial and the periodogram taken). The output of the simulations has a slightly different maximum value for each value of period, but there is no significant dependence of the sensitivity on period; the variation looks like noise and does not maintain repeatable features when the initial random number seed of the full set of randomized trials is changed. Thus we replace the noisy sensitivity level of the simulations with a constant value equal to the average of all the period bins to give the line shown, which is the 99.99 per cent significance threshold for the case of a known period.

The third panel (c) of each figure shows an integral luminosity histogram (the fraction of measurements above each flux value), with the fluxes calculated from the count rates using the PCA

[1] http://lheawww.gsfc.nasa.gov/users/craigm/galscan/main.html

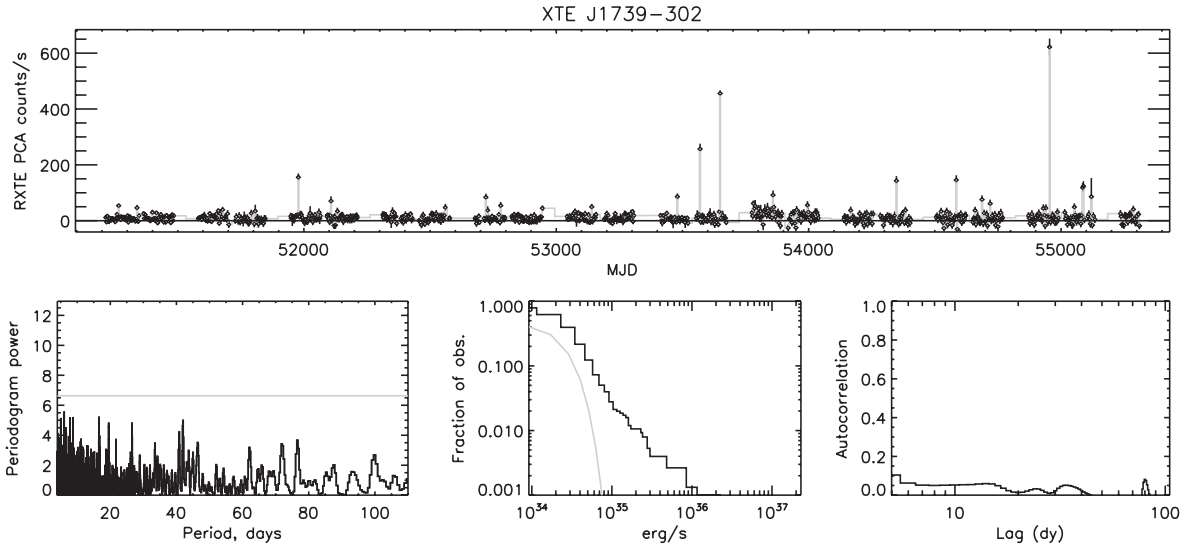

Figure 1. X-ray time-series analysis for XTE J1739−302. Top (panel a): X-ray count rate as a function of time from the bulge scan programme. The rate shown is the equivalent rate for all five proportional counter units (PCUs) summed over the 2–10 keV band, even though fewer detectors were often operating, particularly later in the mission. Bottom-left (panel b): Lomb-normalized periodogram of the data in panel (a). The grey line represents the average maximum value in each period bin in 10^4 randomized trials. Bottom-middle (panel c): histogram of the fraction of samples above a given luminosity as a function of luminosity, using the first-listed distances from Table 1 (see the text). Bottom-right (panel d): autocorrelation function of the data in panel (a).

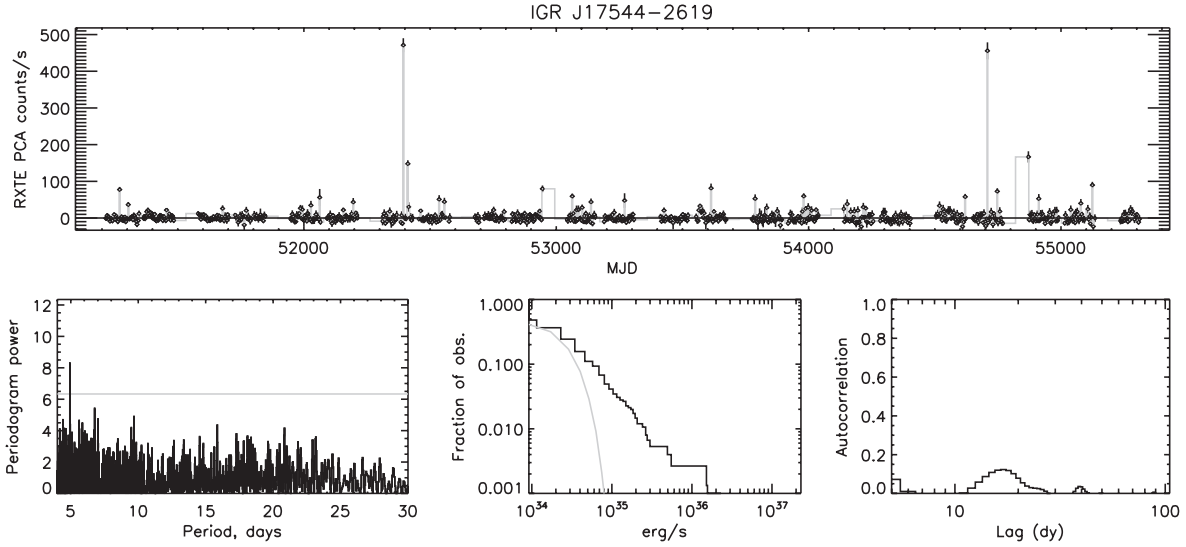

Figure 2. Data products as described in Fig. 1, for IGR J17544−2619.

instrument response and the distances shown in Table 1 (where more than one distance is cited, the first is used). Systems with no good distance estimate (XTE J1901+014 and XTE J1743−363) have been placed at 3 kpc, a distance typical of the estimates for sources that have them. If the nature of these two objects is completely different from that of the supergiant binaries, their distances could be quite different as well. For example, if either is a cataclysmic variable, the distance and luminosity could be much less. Observation of most of these sources in the Galactic bulge is probably due to the region being well observed rather than any physical association with the bulge populations; note that the distances derived for the sources with known companions are all well in the foreground of the Galactic Centre (Table 1). In these panels, the grey lines shown for comparison are the integral of a normal distribution centred at zero whose standard deviation is equal to the average error bar for the lowest 20 per cent of flux observations from each source. This represents the expected distribution if there is no real flux from the source but only random noise.

Finally, the last panel (d) of each figure gives the autocorrelation function of the data for each system. To generate this curve, we interpolated the time history of each system on to a 1d uniform grid, setting all the values to zero during the long gaps that occur each year when the Sun passes too close to the source. The autocorrelation function was calculated on the interpolated grid. Since the source sampling is usually at approximately 3.5 d, these plots are only informative at times longer than that.

In Table 2 we present three different measures of the percentage of time that each source is active. Considering the range of behaviours

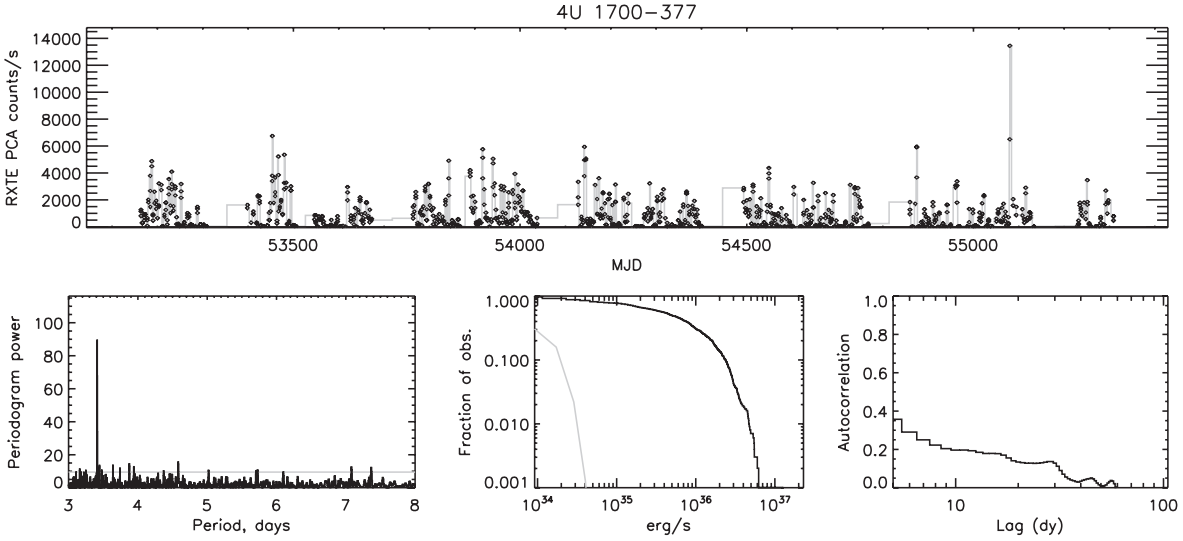

Figure 3. Data products as described in Fig. 1, for 4U 1700−377.

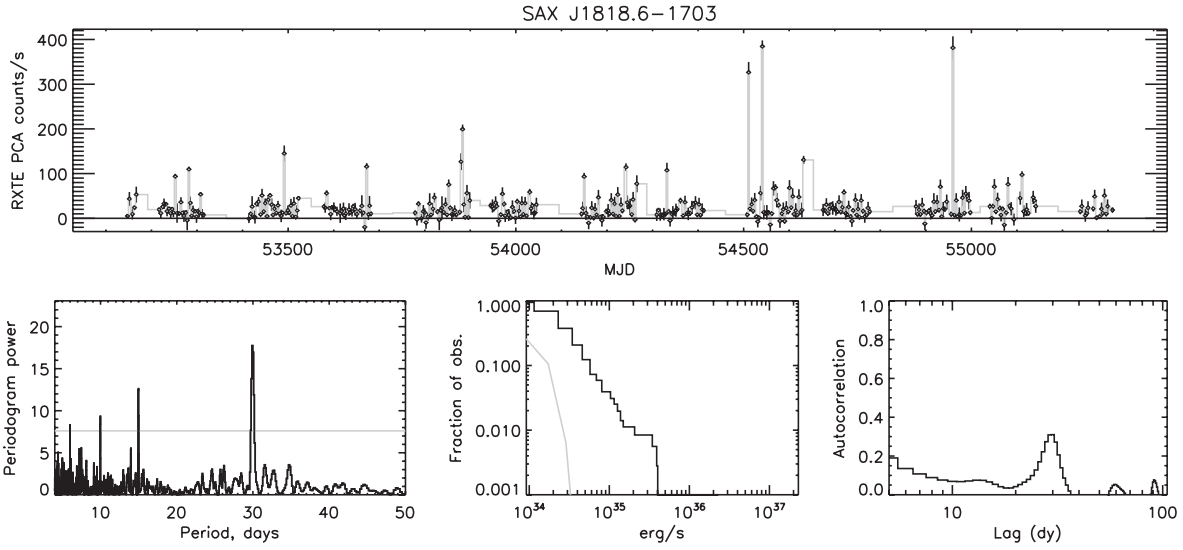

Figure 4. Data products as described in Fig. 1, for SAX J1818.6−1703.

and luminosities among the sources, no single measurement of what it means for a system to be 'active' or 'in outburst' is universally sufficient, nor do we expect one of these three definitions to be useful for every purpose. The first measure is the percentage of time spent with a flux of at least three standard deviations above zero; the standard deviation in this case is defined by averaging the lowest 20 per cent of the error bars from all the bulge scan fits. These errors are partly statistical and partly based on fitting uncertainties from the influence of other nearby sources. In general, the lowest 20 per cent of the errors correspond to times when the source is undetectable to the PCA, with the exception of the sources that are almost always visible, such as 4U 1700−377. The second measure is the percentage time that the source is above 40 counts s^{-1} (2–10 keV, five detectors equivalent), giving a constant threshold in observed flux. The last measure is the percentage of time spent at a luminosity above 1×10^{35} erg s^{-1} at the first listed distance to each source shown in Table 1. Bulge scan count rates (2–10 keV) are converted to energy flux (also 2–10 keV) by assuming a thermal bremsstrahlung spectrum with temperature 20 keV, typical of SFXTs, and using the WEBPIMMS tool at NASA's High Energy Astrophysics Science Archive Research Centre (HEASARC; http://heasarc.nasa.gov/Tools/w3pimms.html, retrieved 2011 April 18). Any of these can be used as a simplified activity parameter, but more information is contained in the full luminosity histograms (panel c of Figs 1–8).

Table 2 also gives the average and maximum luminosity of each source, the average value for the bottom half of luminosity measurements and the average of the bottom 20 per cent of luminosity uncertainties. The latter number serves two purposes: first, to make it clear when the average of the bottom half of luminosity is significantly above zero (only for 4U 1700−377 and XTE J1901+014), and secondly, to give the luminosity threshold used for the first activity index: e.g. XTE J1739−302 spent 4.8 per cent of its time with a flux above $3 \times (2.30 \times 10^{34}$ erg $s^{-1})$. The negative average luminosities for the bottom half of observations in IGR J17544−2619 and IGR J16479−4514 are due to the statistical and systematic

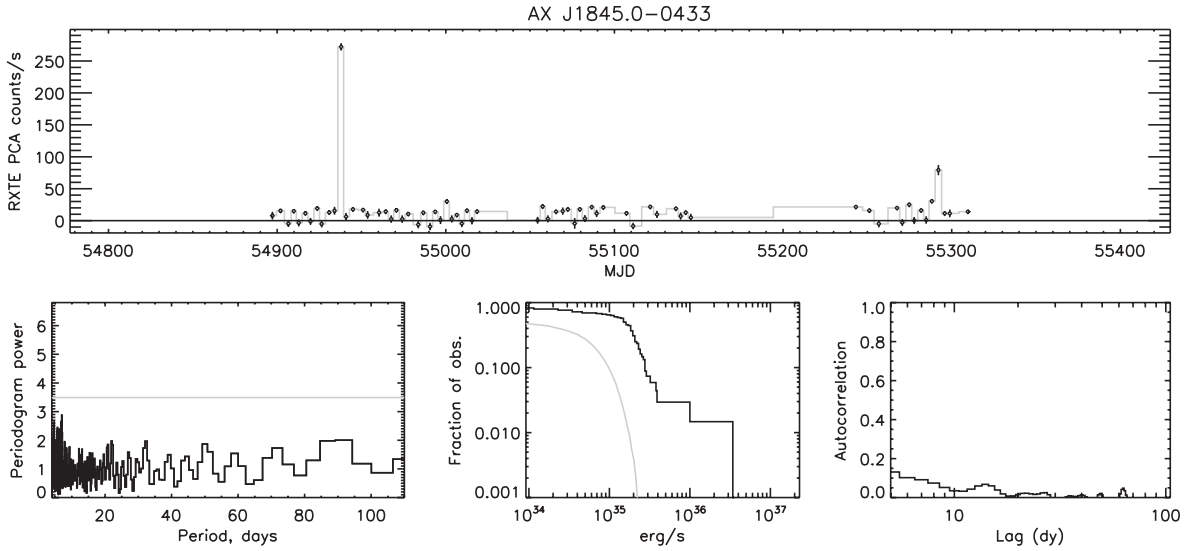

Figure 5. Data products as described in Fig. 1, for AX J1845.0−0433.

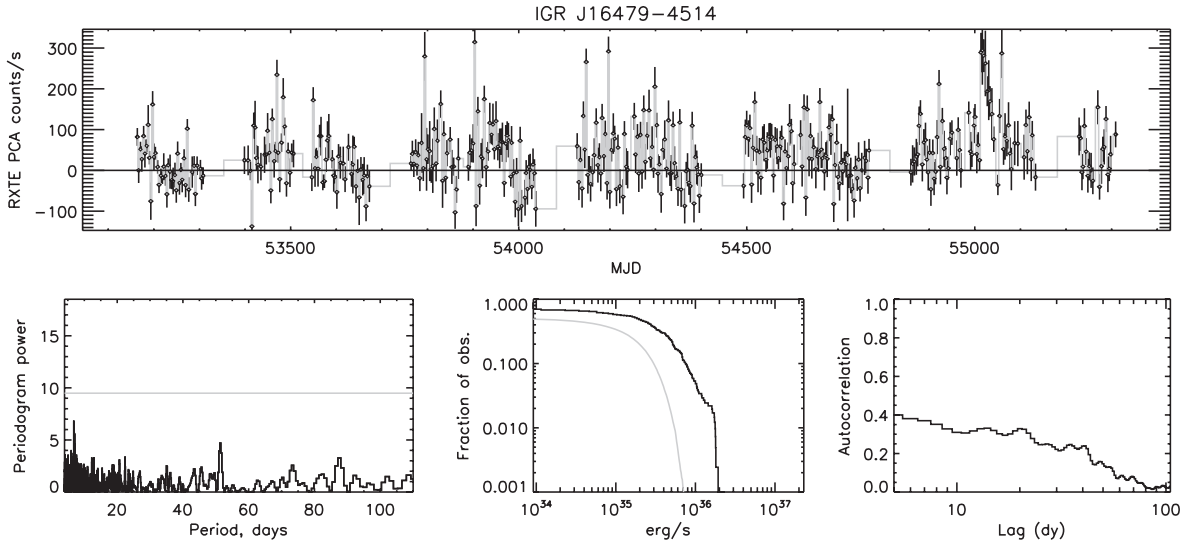

Figure 6. Data products as described in Fig. 1, for IGR J16479−4514.

uncertainties in the background-subtracted PCA count rates. Negative values in these cases just indicate that in a typical measurement, the uncertainties due to subtracting both instrumental background and the influence of other sources are greater than the typical count rate of the source.

Romano et al. (2011) showed luminosity histograms for three sources (differential instead of integral), but summarized these results with an *inactivity* measurement instead. That was most appropriate for their data set, which is only 2 yr long – and therefore contains fewer outbursts – but very sensitive, since the *Swift* XRT is a true imaging instrument. Thus they have good discrimination between low and very low emission levels. The *RXTE* PCA bulge scan data are not as easy to interpret at the lowest fluxes, even though PCA is also very sensitive, due to complications in interpreting the scan data due to the structure of diffuse X-ray emission in the Galactic ridge. On the other hand, the PCA data set contains over 4000 pointings covering over 12 yr for some of the sources we include, so that our data base is the most sensitive to the distribution of the rarer high fluxes.

3 RESULTS AND DISCUSSION

3.1 XTE J1739−302

Drave et al. (2010) recently reported evidence for a 51.47 d period in this system, based on two separate analyses of *INTEGRAL*/IBIS data. In the first, they performed a Lomb–Scargle periodogram on the full IBIS light curve and found the highest power at this period, with a significance greatly exceeding 99.999 per cent confidence. They also collected a number of outbursts from IBIS, *Swift* and *ASCA* data and plotted their frequency of occurrence and intensity with respect to orbital phase, finding that most outbursts occurred around phase 0.5 according to their ephemeris with zero phase defined arbitrarily at MJD 52698.2.

We find no evidence for any power at this period in our periodogram (Fig. 1b), but Drave et al. (2010) pointed out that this was also true of *Swift* and *RXTE* All-Sky Monitor (ASM) data. We note that the PCA bulge scan data presented here have a longer baseline than either *Swift* or *INTEGRAL* and a much higher sensitivity

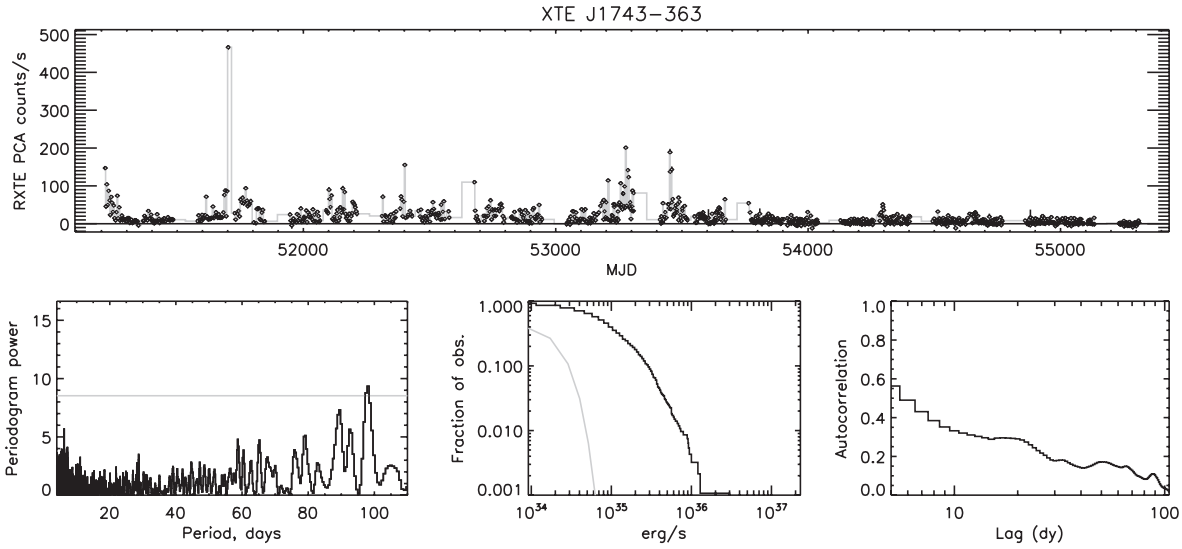

Figure 7. Data products as described in Fig. 1, for XTE J1743−363.

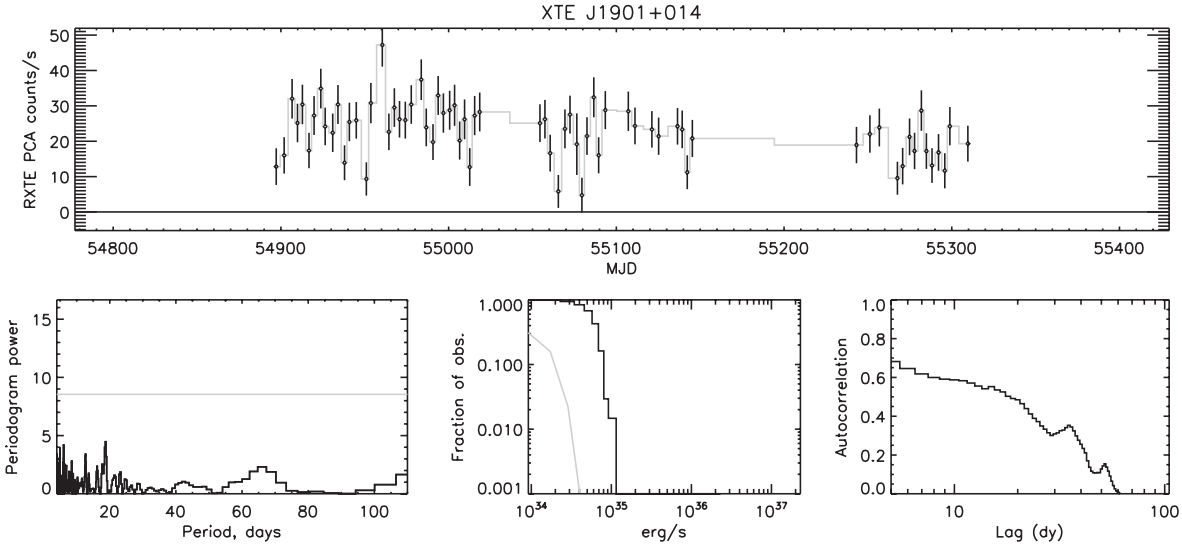

Figure 8. Data products as described in Fig. 1, for XTE J1901+014.

Table 2. X-ray luminosity parameters for eight fast transients.

Name	Per cent $>3\sigma$	Per cent >40 counts s^{-1}	Per cent $>1\times10^{35}$ erg s^{-1}	Average[a]	Average, lower 50 per cent[a]	rms, lower 20 per cent[a]	Maximum[a]
XTE J1739−302	4.8	4.1	2.3	2.25	−0.15	2.30	115.86
IGR J17544−2619	5.8	2.6	3.6	1.25	−2.10	2.41	156.58
4U 1700−377	85.3	84.4	77.1	86.79	15.91	1.16	1240.55
SAX J1818.6−1703	26.4	15.2	3.1	2.58	0.75	0.96	39.40
AX J1845.0−0433	35.5	6.5	68.4	27.00	5.56	7.10	384.19
IGR J16479−4514	11.2	42.3	56.6	22.80	−9.21	23.59	193.66
XTE J1743−363	50.6	10.0	31.4	10.36	1.97	1.97	297.95
XTE J1901+014	83.9	1.9	0.6	5.20	3.85	1.13	10.90

[a] Luminosity in units of 10^{34} erg s^{-1} at the first listed source distance in Table 1, or 3 kpc for XTE J1743−363 and XTE J1901+014.

than the *RXTE* ASM. The twice-weekly monitoring means that the 51.47 d period is very well sampled throughout the 11 yr.

Our result does not, however, necessarily constitute a contradiction of the Drave et al. (2010) result. Each PCA measurement is a snapshot lasting only a few seconds as the spacecraft scans across the source. Most *INTEGRAL* measurements used by Drave et al. (2010), on the other hand, are full 2000 s science windows of that instrument. If we hypothesize that the typical behaviour of the source near periastron is to produce small flares that tend to come at least once every 2000 s but with a duty cycle of <50 per cent, then

it would be plausible that the PCA should miss making positive detections at many periastron transits while *INTEGRAL* might catch most of them.

We therefore turn to the other technique used by Drave et al. (2010), the identification of the phase of medium-to-large outbursts according to the ephemeris they deduced from their periodogram. We have identified 48 outbursts that were not included in the sample given by Drave et al. (2010). These include events from the bulge scans presented here, including some that were presented in Smith et al. (2006), outbursts observed during PCA pointings to 1E 1740.7−2942 given in the same work, *Swift* outbursts from Romano et al. (2009) and one from *INTEGRAL*/IBIS that was not included by Drave et al. (2010). We also include the major outburst observed by *ASCA* in 2002 (MJD 51248.3; Sakano et al. 2002), which was incorrectly assigned a phase of 0.468 by Drave et al. (2010), near the apparent periastron, but was not used in the histogram in their fig. 4, which included 35 events from *INTEGRAL*/IBIS alone. The correct phase of the *ASCA* outburst is 0.83. In many cases, more than one spacecraft observed what was probably the same outburst. Since there is no prescribed way to distinguish one long outburst from two separate ones, we somewhat arbitrarily discarded all new outbursts that were within 1 d of one of those used by Drave et al. (2010), and similarly made sure that no two of the new data points were within 1 d of each other. The new events are given in Table 3.

Table 3. Outbursts of XTE J1739−302 not included by Drave et al. (2010).

MJD	Phase	Major outburst?	Source
50672.7	0.647	Y	*RXTE* pointed
51248.3	0.830	Y	*ASCA*
51849.2	0.505	Y	*RXTE* pointed
51977.9	0.005	Y	*RXTE* scan
52452.9	0.234	Y	*RXTE* pointed
52888.3	0.693	Y	*INTEGRAL*/IBIS
53569.7	0.932	Y	*RXTE* scan
51265.8	0.170	–	*RXTE* scan
51338.5	0.582	–	*RXTE* scan
51660.8	0.844	–	*RXTE* scan
51677.7	0.173	–	*RXTE* scan
52107.5	0.524	–	*RXTE* scan
52560.3	0.321	–	*RXTE* scan
52779.7	0.583	–	*RXTE* scan
52945.1	0.796	–	*RXTE* scan
53140.5	0.594	–	*RXTE* scan
53301.8	0.727	–	*RXTE* scan
53646.1	0.416	–	*RXTE* scan
53649.1	0.475	Y	*RXTE* scan
53781.0	0.038	–	*RXTE* scan
53784.9	0.114	–	*RXTE* scan
53801.8	0.442	–	*RXTE* scan
53847.8	0.335	–	*RXTE* scan
53858.6	0.545	–	*RXTE* scan
53861.5	0.602	–	*RXTE* scan
53995.2	0.200	–	*RXTE* scan
54584.8	0.655	–	*RXTE* scan
54686.9	0.637	–	*RXTE* scan
54719.2	0.266	–	*RXTE* scan
54929.8	0.357	–	*RXTE* scan
54939.8	0.551	–	*RXTE* scan
54954.6	0.840	Y	*RXTE* scan
55052.6	0.742	–	*RXTE* scan
55085.7	0.387	–	*RXTE* scan
55088.6	0.443	–	*RXTE* scan
55286.3	0.284	–	*RXTE* scan
55395.6	0.408	–	*RXTE* scan
55439.9	0.268	–	*RXTE* scan
55453.6	0.533	–	*RXTE* scan
55460.2	0.663	–	*RXTE* scan
53581.0	0.152	–	*Swift*
53663.5	0.755	–	*Swift*
53798.2	0.372	–	*Swift*
54140.7	0.026	–	*Swift*
54632.3	0.577	–	*Swift*
54673.6	0.380	–	*Swift*
54724.5	0.369	–	*Swift*
54900.7	0.792	Y	*Swift*

Fig. 9 shows histograms of outburst phase for the original sample of events used by Drave et al. (2010) the new events, and the sum. The histogram in Fig. 9(a) is identical to that given in fig. 4 of Drave et al. (2010). The new sample, in Fig. 9(b), also peaks near 0.5 in phase. To compare these results to the null hypothesis, we calculated the sum of the squares of the deviations from the average for each plot and compared it to the same quantity for 10^6 simulations of the null hypothesis with the same number of events. The real data sets from panels A, B and C had a sum greater than or equal to all but 5.6, 40.4 and 2.4 per cent, respectively, of the corresponding simulations. This shows that while the new data set provides no evidence for periodicity in its own right, it does increase, and not decrease, the significance of the original result when the samples are combined. Fig. 9(d) shows the phase histogram of the 10 brightest outbursts in the new sample, corresponding to fluxes over 6×10^{-10} erg s^{-1} cm^{-2} or 5×10^{35} erg s^{-1} at 2.7 kpc and marked 'Major' in Table 3. There is no apparent clustering in phase for these events, which include the *ASCA* outburst at phase 0.83, near the minimum occurrence phase for most outbursts.

The integral luminosity distribution at high fluxes (Fig. 1c) has a more or less power-law-like distribution (index of approximately −1.5), a characteristic shared with IGR J17544−2619 (Fig. 2c), the other 'canonical' SFXT system and SAX J1818.6−1703. The autocorrelation function (Fig. 1d) shows no

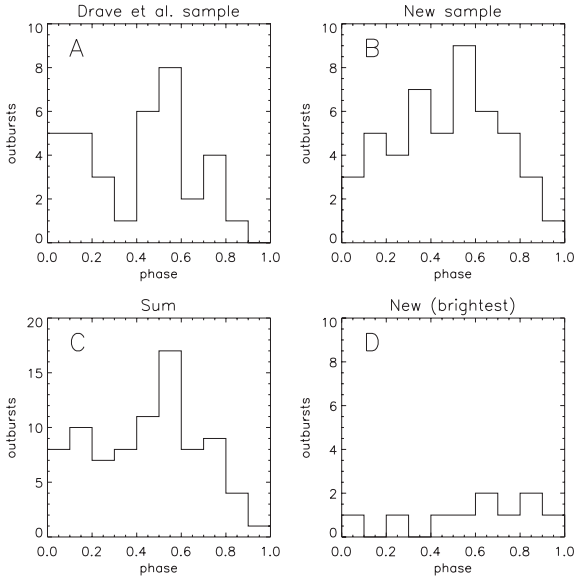

Figure 9. Histograms of outburst phases for XTE J1739−302 according to the ephemeris of Drave et al. (2010). A: outbursts reported by Drave et al. (2010). B: new sample (see the text and Table 3). C: the sum of panels A and B. D: the brightest 10 events in the new sample.

significant signal. If outbursts occur randomly and last for less than the average sampling period (3.5 d), this is to be expected.

3.2 IGR J17544−2619

The orbital period reported by Clark et al. (2009) at 4.926 ± 0.001 d appears clearly in the PCA data (Fig. 2b) at the same period and with comparable error. This signature also appears to a lesser extent in the autocorrelation data (Fig. 2d), where it might be taken for noise if the period were not already known. The intensity distribution and lack of significant autocorrelation of nearby observations look very similar to XTE J1739−302. If there is indeed an order of magnitude difference between the orbital periods of XTE J1739−302 and IGR J17544−2619, it is rather extraordinary that their behaviours are so similar, in frequency of outbursts (shown here), frequency of inactivity (Romano et al. 2011) and in the detailed appearance of the outbursts themselves (e.g. Sidoli et al. 2009). The optical counterparts of IGR J17544−2619 (Pellizza et al. 2006) and XTE J1739−302 (Negueruela et al. 2006; Rahoui et al. 2008) are very similar as well, which argues against an expectation that large differences in the structure and intensity of their winds can compensate for the different orbital radii, producing similar X-ray behaviour. Models that rely on unusual magnetic properties of the neutron star to explain SFXT outbursts (Grebenev & Sunyaev 2007; Bozzo et al. 2008a; Li & Zhang 2011) should be studied further to see if they can produce uniform variability behaviour under greatly differing wind conditions.

3.3 4U 1700−377

This persistently bright wind accretor is shown as a point of comparison for the more transient systems. Its maximum luminosity is higher than that of the two canonical SFXTs discussed above by factors of 11 and 8, but the *average* luminosity is higher by factors of 39 and 69. The comparison of the average luminosity is probably very good, but comparing the maximum luminosity is harder, since we do not know for how long each system tends to stay at this maximum in each outburst, or how common they are. The true maximum level within this 11 yr period may have been missed in one system and caught in another. For example, we know from coverage of one outburst of IGR J17544−2619 by *Suzaku* (Rampy et al. 2009) that the system reached at least 5.3×10^{36} erg s^{-1}. This is as bright as all but one of the data points from the bulge scans of 4U 1700−377. The fast transients are capable of reaching almost the maximum luminosity of this bright system, but spend most of their time at low luminosities.

The well-known orbital period of 4U 1700−377 (see Table 1) is clearly visible, and the autocorrelation function shows coherence on a time-scale of ∼30 d. This could be due to a process intrinsic to the companion star producing slow variations in its wind, a feedback between the accretion luminosity of the neutron star and mass loss from the companion, or the presence of an accretion disc around the neutron star, with a viscous time-scale of this order.

3.4 SAX J1818.6−1703

This system (in't Zand et al. 1998) looks similar to the two canonical SFXTs in terms of the power-law shape of the distribution of luminosities (Fig. 4c). The orbital period (see Table 1) and its harmonics are clearly seen in the periodogram; even the autocorrelation function shows a correlation at the orbital period, which we believe represents the high probability of an unrelated outburst at the next periastron passage. Sidoli et al. (2009) found that the outbursts of this system, studied in depth with *Swift*, show very similar characteristics to the canonical SFXTs. Its 30 d orbital period is approximately half-way between those of IGR J17544−2619 and XTE J1739−302, showing again that very similar outburst duty cycles and luminosities are seen with different orbital parameters. While the system has been shown to have as deep a quiescence as the canonical SFXTs (Bozzo et al. 2008b), there has not been enough monitoring by a sensitive telescope such as *Swift* to get the good data on frequency of quiescence that are now available for other systems (Romano et al. 2011).

3.5 AX J1845.0−0433 and IGR J16479−4514

There was only one major and one minor outburst of AX J1845.0−0433 caught by the bulge scans, as can be seen in Fig. 5, panel (a), and no obvious outburst of IGR J16479−4514. The contamination of AX J1845.0−0433 by Galactic plane diffuse emission, visible as a bifurcation between those scans taken perpendicular and parallel to the plane, makes any conclusion about the flux outside of outbursts difficult; the contamination of IGR J16479−4514 by GX 340+0 produces a similar problem. While both of these sources show a fairly high average luminosity in the fifth column of Table 2, we do not claim this result as significant; repeated observations with a focusing instrument such as the *Swift* XRT would be preferable to establish the quiescent and low-flux behaviour of these sources.

3.6 XTE J1743−363

3.6.1 Position and identification

This source was discovered by Markwardt, Swank & Marshall (1999). Its occasional fast outbursts have led to the suggestion that it might be an SFXT, and the X-ray spectrum in outburst could be fitted with a thermal bremsstrahlung spectrum with temperature 22 keV, typical of X-ray pulsars and SFXTs (Sguera et al. 2006). Ratti et al. (2010), using a *Chandra* observation of the field (2008 February 8, principal investigator MM), identified a cluster of 11 X-ray photons corresponding to the position of the bright infrared (IR) source 2MASS 17430133−3622221. This is the only significant source in the *Chandra* field, although it is possible that XTE J1743−363 was entirely quiescent at that time and the X-rays come from another system. Fig. 10 compiles some X-ray position measurements for XTE J1743−363: the initial *RXTE* estimate at the source's discovery (Markwardt et al. 1999; at 10 arcmin, its error circle is too large to appear on the plot), the most precise *INTEGRAL*/IBIS position (0.7 arcmin error circle, 90 per cent confidence; Bird et al. 2010), the *Swift* BAT position from the 58 month catalogue (Baumgartner et al. 2010), the *Chandra* position (Ratti et al. 2010) and our new, refined *RXTE* position. Earlier *Swift*/BAT positions, while different, are consistent with both the newest BAT position and the *Chandra* source (Cusumano et al. 2010; Tueller et al. 2010).

The *RXTE* position was derived from a dedicated scan of the source using the PCA instrument. The observation was made on 1999 February 15 at 01:15 UT for 2.4 ks. The scan pattern consisted of a connected path, including scans along constant right ascension and declination. The model included XTE J1743−363 and one other known source in the field of view, 4U 1746−37, at a fixed position. The primary change in deriving the refined position was that the intensity of XTE J1743−363 was allowed to vary with a long-term linear trend. The uncertainties of individual measurements were

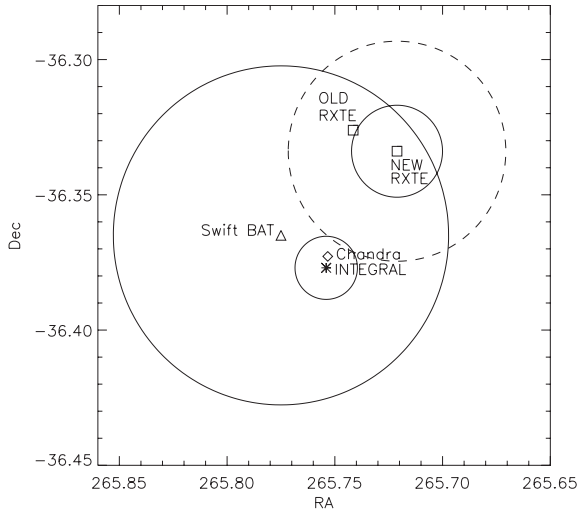

Figure 10. Summary of position measurements for XTE J1743−363. The *Chandra* position has too small an error circle to be plotted on this scale, and the first *RXTE* position has too large a circle. The new *RXTE* position is shown with the 3σ contour (dashed line) as well as the 1σ contour (solid line). See the text.

increased in order to deweight the strong variability of the source, which was near 35 per cent rms. While the *Chandra* position is slightly outside the 3σ *RXTE* contour, the susceptibility of the *RXTE* fit to variability, combined with the agreement of *INTEGRAL*/IBIS with *Chandra* (spanning both the low- and high-energy ends of the PCA energy range), leads us to conclude that all the observatories are seeing the same source.

3.6.2 X-ray characteristics

In hopes of getting further insight into the nature of this source, we examined 12 archived *RXTE*/PCA pointings, some from 2000, when it was often bright, and some from 2007, when it was much less active (see Fig. 7). Table 4 shows the dates, *RXTE* observation identification numbers and count rates for these pointings. Fig. 11 shows some sample light curves and Fig. 12 shows the power spectrum made by averaging the power spectra from five of the observations.

Four observations made on MJD 54115 showed low and nearly identical count rates of 1.9–2.0 counts s^{-1} and no variability. The flux varied during all the other observations on time-scales of seconds to minutes. We used XSPEC version 12.5.1 to fit the PCA spectra. These four quiet observations included an iron line of high equivalent width, and no detectable interstellar absorption above 3 keV, in contrast to all the other observations, which showed significant and variable absorption. Finally, the count rates of the four spectra from MJD 54115 are comparable to the flux level that is identified as diffuse from the PCA bulge scans in this region. Taking all this evidence together, we believe it quite likely that during these four observations we were seeing only the Galactic diffuse component and not the source itself. The best-fitting continuum spectrum to these four observations together was an optically thin thermal bremsstrahlung spectrum of temperature 10.10 ± 0.50 keV and normalization $(5.99 \pm 0.16) \times 10^{-3}$, defined as

$$\frac{3.02 \times 10^{-15}}{4\pi D^2} \int n_{\rm e} n_{\rm I}\, {\rm d}V, \qquad (1)$$

where D is the distance to the source in centimetres and $n_{\rm e}$ and $n_{\rm I}$ are the electron and ion densities per cubic centimetre at the source (Arnaud et al. 2011). An iron line of equivalent width 0.43 keV and centre energy (6.63 ± 0.54) keV was also required (at 3.7σ), and was consistent with being narrow, although the width was poorly constrained (<2.9 keV). In fitting the rest of the spectra, we included these two spectral components with no free parameters. No further iron line was needed in any of the other fits.

In Table 4 we show the spectral parameters of the remaining flux, presumed to be from XTE J1743−363 itself. For most of the spectra, an absorbed optically thin thermal bremsstrahlung spectrum provided a good fit. We used the Tuebingen–Boulder interstellar medium absorption model (Wilms, Allen & McCray 2000). For the three spectra with the best counting statistics, however, an additional component was necessary to obtain χ^2 values consistent with chance. A thermal blackbody spectrum served this purpose well for all three spectra, as it typically does for accreting neutron stars. Table 5 shows the resulting fit parameters in this case. Including the blackbody component has the effect of raising the temperature of the bremsstrahlung component and reducing the best-fitting absorption column.

It is apparent from Tables 4 and 5 that the absorption column is both high and variable, and therefore local to the system. This

Table 4. List of PCA pointings to XTE J1743−363 and absorbed bremsstrahlung fits.

Observation ID	MJD	Rate[a]	nH[b]	kT (keV)	Normalization[c]
40408-01-01-00	51224.051	12	11.05 ± 0.22	13.76 ± 0.35	5.509 ± 0.082
40408-01-02-00	51230.781	22	6.11 ± 0.16	13.67 ± 0.34	8.24 ± 0.11
50138-02-01-00	51706.236	23	17.40 ± 0.43	14.66 ± 0.54	11.44 ± 0.27
50138-02-02-00	51707.631	13	10.55 ± 0.51	15.74 ± 0.97	4.64 ± 0.15
50138-02-03-00	51710.759	11	10.26 ± 0.66	11.42 ± 0.77	4.33 ± 0.20
50138-02-04-00	51713.016	11	8.77 ± 0.53	10.54 ± 0.58	4.01 ± 0.16
92047-04-01-02	54115.404	2.0	–	–	–
92047-04-01-04	54115.461	2.0	–	–	–
92047-04-01-00	54115.520	1.9	–	–	–
92047-04-01-01	54115.910	1.9	–	–	–
92047-04-02-00	54301.307	5.3	11.6 ± 1.4	14.5 ± 2.2	1.57 ± 0.14
92047-04-02-01	54303.272	3.2	7.4 ± 1.7	15.9 ± 3.8	0.503 ± 0.076
92047-04-02-02	54304.383	3.2	8.4 ± 1.6	16.4 ± 3.7	0.550 ± 0.075

[a] counts s^{-1}/PCU.
[b] $\times 10^{22}$ cm^{-2}.
[c] $\times 10^{-2}$ as defined in equation (1).

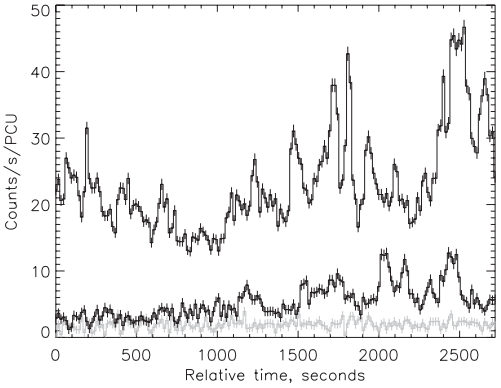

Figure 11. X-ray variability at three representative luminosities of XTE J1743−363. Top trace: observation 50138-02-01-00. Middle trace: observation 92047-04-02-00. Bottom trace (grey): observation 92047-04-01-00. See Table 4.

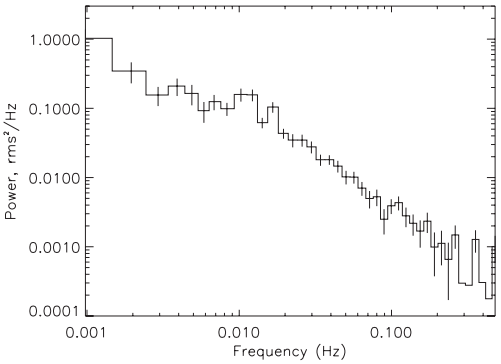

Figure 12. Power spectrum combining the data from observations 40408-01-02-00, 50138-02-01-00, 50138-02-02-00, 50138-02-03-00 and 50138-02-04-00. No pulse period is visible between 2 and 1024 s.

suggests a companion with a dense wind, which can be characteristic of both blue supergiants and red giants such as AGB stars. The absorption column does not seem to correlate with luminosity at all, suggesting that the absorption is taking place in foreground structures in the wind rather than in the concentration of material accreting on to the compact object at the moment.

3.6.3 Optical spectroscopy

Ratti et al. (2010) used the IR colours of 2MASS 17430133–3622221 to constrain the spectral type of the companion, but not severely; they found that a giant of type G0–6, a G or K supergiant, or a supergiant earlier than O9 were all consistent with the Two Micron All Sky Survey (2MASS) colours, assuming varying degrees of reddening. The 2MASS magnitudes are $J = 9.616$, $H = 8.305$ and $K = 7.624$. The 2MASS source (Fig. 13) is coincident with USNO–B1.0 0536–0518280, with $R = 16.4$ and 16.77 (R1 and R2 measurements) and $I = 13.78$ (not seen in the USNO B band) and with the Midcourse Space Experiment IR source MSX6C G353.3697−03.4195, seen only in band A at 0.1386 Jy. Band A is centred at 8.28 μm with half-maximum points at 6.8 and 10.8 μm according to Egan et al. (2003).

We obtained a far-red spectrum of the counterpart using the Andalucia Faint Object Spectrograph and Camera (ALFOSC) on the 2.6-m Nordic Optical Telescope (NOT) in La Palma, Spain, on the night of 2009 June 27. The instrument was equipped with a thin 2048 × 2048 pixel E2V CCD, covering a field of view of 6.4×6.4 arcmin^2 with a spatial scale 0.19 arcsec pixel^{-1}. We used grism #4 with a 1.0 arcsec slit, providing a resolving power $R \approx 450$. In order to remove fringing, an internal flat was taken at the target position.

Because of the Southern declination of the target, it was observed at a very high airmass ($Z = 2.4$). However, as the finder image (Fig. 14) shows, image quality was good. 2MASS J17430133−3622221 can be clearly resolved into two objects, separated by ∼2arcsec, both of which fell within the slit. The fainter object is a normal G/K star. The brighter star is a very red object, and the obvious counterpart to the 2MASS source. Its spectrum (Fig. 15) is dominated by deep molecular bands. In particular, we see deep bandheads of TiO, typical of M-type stars.

Negueruela et al. (2011) have shown that the depth of the TiO 8859 Å bandhead is a very good indicator of effective temperature. Though the resolution of our spectrum is too low to use it as a $T_{\rm eff}$ calibrator, the fact that its depth is $\gtrsim$0.5 of the continuum immediately shortward indicates that it is not a dwarf star. Only giants and supergiants present such deep molecular features. It also indicates that the spectral type is later than M6. This is confirmed by the detection of VO bandheads, which are only visible at spectral types M7 and later (Turnshek et al. 1985; Gray & Corbally 2009).

The deep depression of the continuum in the 7400–7550 and 7860–8050 Å regions can only be due to the presence of strong VO bands of the extreme red system, as there are no telluric features in these two regions. Moreover, the VO bandhead at 8624 Å is also likely detected. Though a better spectrum is needed to obtain an accurate spectral type, the data are not very different from the expectation for spectral type M8. As supergiants with such a late spectral type are very rare (Levesque et al. 2005), the object is very likely a giant.

The fundamental properties of such late stars are not well calibrated. For M8 III stars, van Belle et al. (1999) estimate $T_{\rm eff} = 3050$ K, though this is an extrapolation from earlier spectral types. Their fit to the intrinsic $(V - K)_0$ colour indicates values between $(V - K)_0 = -8.0$ and $(V - K)_0 = -8.5$ at this temperature. As Thé et al. (1990) find $M_V = +1.6$ on average for M8 III giants, their IR absolute magnitude is $M_K \lesssim -6.4$. Late M-type giants may be close to tip of the red giant branch (RGB) or on the asymptotic giant branch (AGB). Many giants later than M6 are brighter than the tip

Table 5. Absorbed bremsstrahlung plus blackbody fits to XTE J1743−363 spectra.

Observation ID	nH[a]	Bremss. kT (keV)	Bremss. norm.[b]	Blackbody kT (keV)	Blackbody norm.[c]
40408-01-01-00	8.52 ± 0.47	29.5 ± 6.7	3.09 ± 0.30	1.673 ± 0.042	0.79 ± 0.23
40408-01-02-00	3.69 ± 0.42	23.5 ± 4.5	4.67 ± 0.50	1.801 ± 0.050	1.21 ± 0.33
50138-02-01-00	13.44 ± 0.86	24.9 ± 6.2	6.15 ± 0.89	2.058 ± 0.085	1.82 ± 0.54

[a] $\times 10^{22}$ cm^{-2}.
[b] $\times 10^{-2}$ as defined in equation (1).
[c] $\times 10^{-3}$ normalized to 10^{39} erg s^{-1} at 10 kpc (Arnaud, Dorman & Gordon 2011).

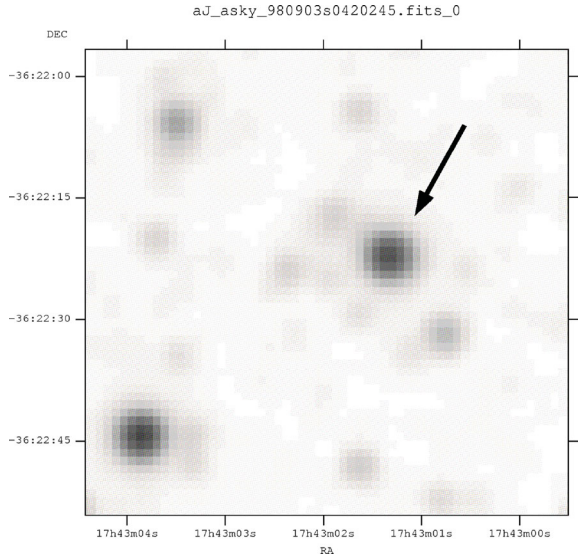

Figure 13. 2MASS *J*-band image of the region around 2MASS 17430133–3622221. The arrow marks the source.

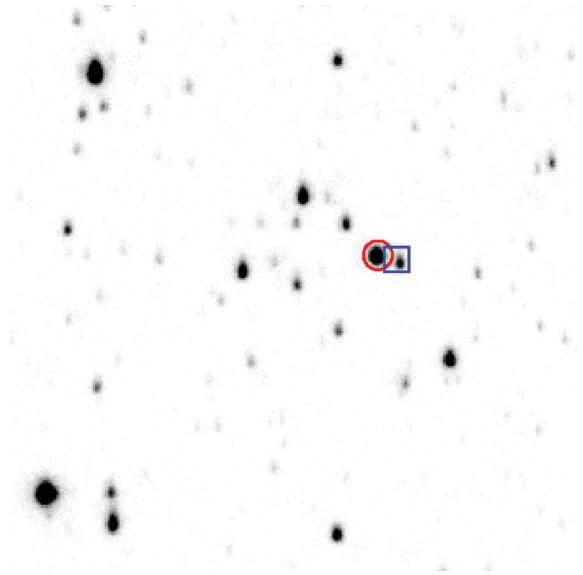

Figure 14. NOT finder image covering the same area as Fig. 13. Note that 2MASS 17430133–3622221 is resolved into two sources. The brighter source to the left (marked with a circle) is the M giant discussed in the text.

of the RGB (e.g. Tabur et al. 2009a), which has observationally been set at $M_K = -6.85$ (Tabur, Kiss & Bedding 2009b), and so most M8 III giants are likely on the AGB.

Theoretical magnitudes calculated from PHOENIX models and calibrated against observational data suggest that all late M giants have $(J - K)_0 \sim 1.3$ (Kučinskas et al. 2005), in good agreement with extrapolation of the colour calibration of Straižys & Lazauskaitė (2009). The calibration of Groenewegen (2004), based on older models, gives $(J - K)_0 = 1.37$ for dust-free M8 stars. This reference also gives $(J - K)_0 = 1.97$ for dust-enshrouded M7 stars. Based on this, our target cannot be dust enshrouded, unless the interstellar extinction is negligible. This possibility is ruled out by the non-detection in all MSX bands except for A, and so we assume that the star is not surrounded by dust. Therefore its colour excess is $E(J - K)_0 \approx 0.6$–0.7. For a standard reddening law, $A_K \approx 0.4 - 0.5$ and so the distance modulus should be DM ≈ 13.5, i.e. $d \approx 5$ kpc. As observations of Large Magellanic Cloud giants suggest that M_K may deviate by ± 0.6 mag from the average at a given $(J - K)$ (Cioni et al. 2001), we may settle for $d \approx 5 \pm 1$ kpc, though there are many other sources of uncertainty not considered in this error estimate.

For instance, these calculations assume that the star has characteristics typical of M-type giants in the solar neighbourhood. Our upper limit on the distance to the source, however, places it close to the Galactic Bulge. At $b = -3.^{\circ}4$, the extinction to our source is not incompatible with Galactic bulge membership (Dutra et al. 2003), even if we take into account the possibility of bluer colours for bulge M giants (Frogel 1988). However, for a distance of 8.5 kpc, the source would have $M_{K_S} \approx -7.8$, only compatible with the very brightest bulge M-type stars (Glass & Schultheis 2002). Our target would then have to be a thermally pulsating AGB.

Even in the most likely case that the star is foreground to the bulge, it is likely to be variable, as most late-type giants are long-period variables. Their amplitude in the *K* band is generally small and unlikely to dominate our error budget. On the other hand, photometric determination of a pulsation period would be the most direct way to evaluate the stellar luminosity and hence distance.

3.6.4 XTE J1743−363 as a symbiotic X-ray binary

The spectral identification of the companion to XTE J1743−363 as a late M giant puts the system in the small group of symbiotic X-ray binaries, although we have not seen an additional hot component to the optical spectrum, which was the origin of the term 'symbiotic'. For comparison, we show in Fig. 16 the PCA bulge scan data for GX 1+4, a known symbiotic X-ray binary in which an X-ray pulsar orbits an M giant. Hinkle et al. (2006) used IR spectroscopy to derive an orbital period of 1161 d, a luminosity of 1270 $L_{\odot}$ and a distance of 4.3 kpc, which we assume to scale the luminosity distribution in Fig. 16. Comparing GX 1+4 with the data for XTE J1743−363 in Fig. 7, we see two things in common: a notable autocorrelation out to 100 d (while even the very bright blue supergiant system 4U 1700−377 only correlates out to 30 d) and a long quiet period (for GX 1+4, the years 2007 and 2008 and for XTE J1743−363 the last 5 yr). These common characteristics lend support to the spectroscopic evidence that XTE J1743−363 is also a symbiotic binary. Strong emission lines in the optical spectrum and pulsations of GX 1+4 have been taken as evidence of an accretion disc (Chakrabarty & Roche 1997; Jablonski et al. 1997). While these characteristics have not been seen in XTE J1743−363, we note that our far-red spectrum of XTE J1743−363 was taken in the middle of the extended X-ray quiet period still in progress. It is possible that a disc forms when the source is X-ray active.

The time variability of XTE J1743−363 also resembles that of a member of another class of binary entirely: the ultracompact binary 4U 0513−40 in globular cluster NGC 1851. It also shows highly variable emission, correlations over many days, and a relatively quiet period of ∼3 yr (Maccarone et al. 2010). Our spectroscopy of the counterpart rules out this possibility, unless the correct companion is the faint, non-descript G/K star nearby. It is unlikely, however, that a star as unusual as the M8 giant would coincide with the X-ray source by accident, while it is quite likely that the dwarf star would do so.

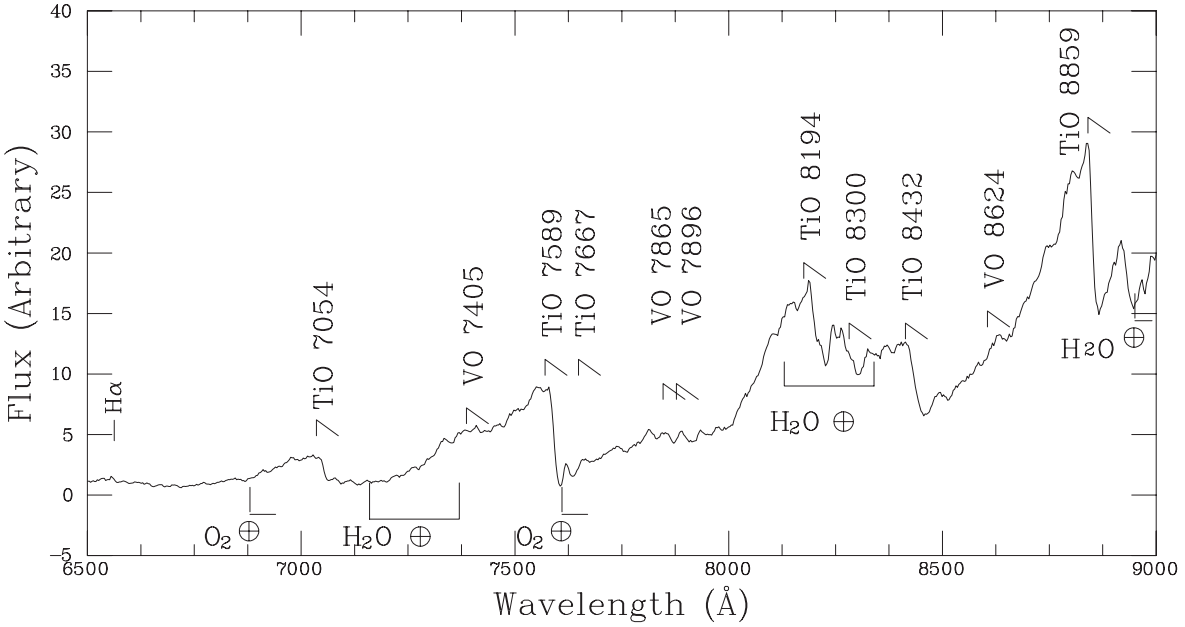

Figure 15. ALFOSC spectrum of 2MASS 17430133–3622221/USNO–B1.0 0536–0518280. The positions of some relevant molecular bandheads are indicated. The strongest telluric features are also marked.

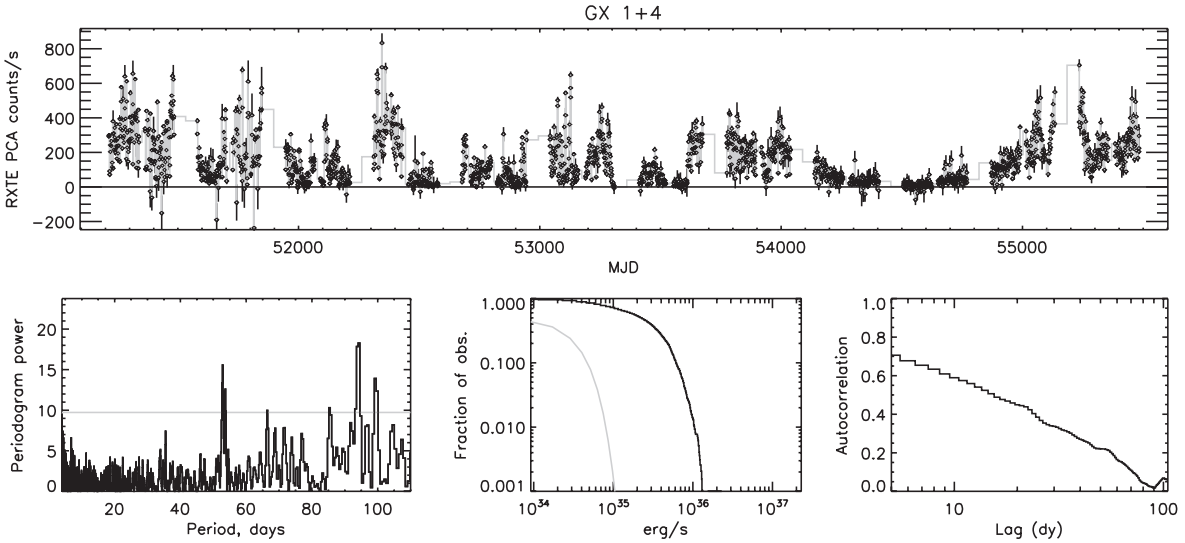

Figure 16. Data products as described in Fig. 1, for the symbiotic binary GX 1+4.

3.7 XTE J1901+014

This system showed a short (<3.15 h), bright (0.9 Crab) X-ray outburst at the time of its discovery by Remillard & Smith (2002). It has since shown further outbursts (Krimm et al. 2010) but seems to have a relatively high flux in quiescence as well (Karasev, Lutovinov & Grebenev 2007; Karasev et al. 2008) compared to the SFXTs (Smith et al. 2007; Krimm et al. 2010). It does not have an IR/optical counterpart bright enough to be a supergiant in our Galaxy (Smith et al. 2007; Karasev et al. 2008). Although we did not see an outburst in the bulge scan data, we confirm the presence of a non-zero quiescent baseline that is not consistent with the behaviour of the SFXTs in our sample. Karasev et al. (2007), using pointed observations of the *RXTE* PCA, showed that there is a great deal of variability (by more than a factor of 2 over tens of seconds) even outside of outbursts. They quoted a typical flux of 2.7 mCrab outside of outburst. Our average luminosity of 5.72×10^{34} erg s^{-1} at an arbitrary distance of 3 kpc corresponds to 5.3×10^{-11} erg s^{-1} or a bit over 2 mCrab, in agreement with Karasev et al. (2007). The persistent emission outside of outburst supports the more definitive evidence of the lack of a supergiant companion in separating this source from the class of SFXTs. The nature of the system remains a mystery.

ACKNOWLEDGMENTS

The authors thank Sebastian Drave for his assistance in identifying an independent set of outbursts of XTE J1739−302 from those used in Drave et al. (2010) and for useful discussions. DMS would also like to thank Tom Maccarone for stimulating discussions on the interpretation of the XTE J1743−363 data. We thank the referee

for many perceptive comments and for catching a number of minor errors.

The 2MASS image (Fig. 13) was retrieved from the NASA/IPAC IR Science Archive, which is operated by the Jet Propulsion Laboratory, California Institute of Technology, under contract with the National Aeronautics and Space Administration.

Our results on XTE J1743−363 were partially based on observations made with the Nordic Optical Telescope, operated on the island of La Palma jointly by Denmark, Finland, Iceland, Norway and Sweden, in the Spanish Observatorio del Roque de los Muchachos of the Instituto de Astrofisica de Canarias. The data presented here (Figs 14 and 15) have been taken using ALFOSC, which is owned by the Instituto de Astrofisica de Andalucia (IAA) and operated at the Nordic Optical Telescope under agreement between IAA and the Niels Bohr Institute for Astronomy, Physics and Geophysics (NBIfAFG) of the Astronomical Observatory of Copenhagen.

IN is partially supported by the Spanish Ministerio de Ciencia y Tecnología under grants AYA2010-21697-C05-05 and CSD2006-70.

REFERENCES

Ankay A., Kaper L., de Bruijne J. H. J., Dewi J., Hoogerwerf R., Savonije G. J., 2001, A&A, 370, 170

Arnaud K., Dorman B., Gordon C., 2011, XSPEC User's Guide for version 12.7.0, http://heasarc.nasa.gov/xanadu/xspec/manual/manual.html, accessed 2011 October 17

Baumgartner W. et al., 2010, ApJ, submitted, http://heasarc.nasa.gov/docs/swift/results/bs58mon/, accessed 2011 October 17

Bird A. J., Bazzano A., Hill A. B., McBride V. A., Sguera V., Shaw S. E., Watkins H. J., 2009, MNRAS, 393, L11

Bird A. J. et al., 2010, ApJS, 186, 1

Bozzo E., Falanga M., Stella L., 2008a, ApJ, 683, 1031

Bozzo E., Campana S., Stella L., Falanga M., Israel G., Rampy R., Smith D. M., Negueruela I., 2008b, Astron. Telegram, 1493

Chakrabarty D., Roche P., 1997, ApJ, 489, 254

Chaty S., 2010, in Marti J., ed., ASP Conf. Ser. Vol. 422, High Energy Phenomena in Massive Stars. Astron. Soc. Pac., San Francisco, p. 243

Cioni M.-R. L. et al., 2001, A&A, 377, 945

Clark D. J., Hill A. B., Bird A. J., McBride V. A., Scaringi S., Dean A. J., 2009, MNRAS, 399, L113

Clark D. J. et al., 2010, MNRAS, 406, 75

Coe M. J., Fabregat J., Negueruela I., Roche P., Steele I. A., 1996, MNRAS, 281, 333

Cusumano G. et al., 2010, A&A, 510, 48

Drave S. P., Clark D. J., Bird A. J., McBride V. A., Hill A. B., Sguera V., Scaringi S., Bazzano A., 2010, MNRAS, 409, 1220

Dutra C. M., Santiago B. X., Bica E. L. D., Barbuy B., 2003, MNRAS, 338, 253

Egan M. P. et al., 2003, VizieR On-line Data Catalog: V/114. Originally published in Air Force Research Laboratory Technical Report, AFRL-VS-TR-2003-1589

Frogel J. A., 1988, ARA&A, 26, 51

Glass I. S., Schultheis M., 2002, MNRAS, 337, 519

Gray R. O., Corbally C. J., 2009, Stellar Spectral Classification. Princeton Univ. Press, Princeton

Grebenev S. A., Sunyaev R. A., 2007, Astron. Lett., 33, 149

Groenewegen M. A. T., 2004, A&A, 425, 595

Hinkle K. H., Fekel F. C., Joyce R. R., Wood P. R., Smith V. V., Lebzelter T., 2006, ApJ, 641, 479

Hong J., Hailey C. J., 2004, ApJ, 600, 743

in't Zand J. J. M., 2005, A&A, 441, 1

in't Zand J., Heise J., Smith M., Muller J. M., Ubertini P., Bazzano A., 1998, IAU Circ., 6840

Jablonski F. J., Pereira M. G., Braga J., Gneiding C. D., 1997, ApJ, 482, L171

Jahoda K. et al., 2006, ApJS, 163, 401

Jain C., Paul B., Dutta A., 2009, MNRAS, 397, L11

Karasev D. I., Lutovinov A. A., Grebenev S. A., 2007, Astron. Lett., 33, 159

Karasev D. I., Lutovinov A. A., Burenin R. A., 2008, Astron. Lett., 34, 753

Krimm H. A. et al., 2010, Astron. Telegram, 2375

Kučinskas A. et al., 2005, A&A, 442, 281

Levesque E. M., Massey P., Olsen K. A. G., Plez B., Josselin E., Maeder A., Meynet G., 2005, ApJ, 628, 973

Li X.-D., Zhang Z., 2011, MNRAS, 418, 556

Maccarone T. J., Long K. S., Knigge C., Dieball A., Zurek D. R., 2010, MNRAS, 406, 2087

Markwardt C. B., Swank J. H., Marshall F. E., 1999, IAU Circ., 7120, 1

Megier A., Strobel A., Galazutdinov G. A., Krełowski J., 2009, A&A, 507, 833

Negueruela I., Schurch M. P. E., 2007, A&A, 461, 631

Negueruela I., Smith D. M., Reig P., Chaty S., Torrejón J. M., 2006, in Wilson A., ed., ESA SP-604: The X-ray Universe 2005. ESA, Noordwijk, p. 165

Negueruela I., Smith D. M., Torrejon J. M., Reig P., 2007, in Grebenev S., Sunyaev R., Winkler C., eds, ESA SP-622: The Obscured Universe 2006. ESA, Noordwijk, p. 255

Negueruela I. et al., 2008a, Bandyopadhyay R. M., Wachter S., Gelino D., Gelino C. R., eds, AIP Conf. Ser. Vol. 1010, A Population Explosion: The Nature and Evolution of X-Ray Binaries in Diverse Environments. Am. Inst. Phys., New York, p. 252

Negueruela I., Torrejón J. M., Reig P., 2008b, in Proc. 7th *INTEGRAL* Workshop, Copenhagen, Denmark, PoS(Integral08)072

Negueruela I., González-Fernández C., Marco A., Clark J. S., 2011, A&A, 528, A59

Nespoli E., Febregat J., Mennickent R. E., 2008, A&A, 486, 911

Pellizza L. J., Chaty S., Negueruela I., 2006, A&A, 455, 653

Rahoui F., Chaty S., Lagage P.-O., Pantin E., 2008, A&A, 484, 801

Rampy R. A., Smith D. M., Negueruela I., 2009, ApJ, 707, 243

Ratti E. M., Bassa C. G., Torres M. A. P., Kuiper L., Miller-Jones J. C. A., Jonker P. G., 2010, MNRAS, 408, 1866

Remillard R., Smith D. A., 2002, Astron. Telegram, 88

Revnivtsev M., Sazonov S., Gilfanov M., Churazov E., Sunyaev R., 2006, A&A, 452, 169

Romano P. et al., 2009, MNRAS, 399, 2021

Romano P. et al., 2011, MNRAS, 410, 1825

Romano P. et al., 2012, MNRAS, 419, 2695

Sakano M., Koyama K., Murakami H., Maeda Y., Yamauchi S., 2002, ApJS, 138, 19

Sguera V. et al., 2005, A&A, 444, 221

Sguera V. et al., 2006, ApJ, 646, 452

Sguera V., Drave S. P., Bird A. J., Bazzano A., Landi R., Ubertini P., 2011, MNRAS, 417, 573

Sidoli L. et al., 2007, A&A, 476, 1307

Sidoli L. et al., 2009, MNRAS, 397, 1528

Smith D. M., 2003, Astron. Telegram, 184

Smith D. M., 2004, Astron. Telegram, 338

Smith D. M., Main D., Marshall F., Swank J., Heindl W. A., Leventhal M., in't Zand J. J. M., Heise J., 1998, ApJ, 501, L181

Smith D. M., Heindl W. A., Markwardt C. B., Swank J. H., Negueruela I., Harrison T. E., Huss L., 2006, ApJ, 638, 974

Smith D. M., Rampy R. A., Negueruela I., Torrejón J. M., 2007, Astron. Telegram, 1268

Straižys V., Lazauskaitė R., 2009, Baltic Astron., 18, 19

Swank J. H., Markwardt C. B., 2001, in ASP Conf. Ser. Vol. 251, New Century of X-ray Astronomy. Astron. Soc. Pac., San Francisco, p. 94

Tabur V., Bedding T. R., Kiss L. L., Moon T. T., Szeidl B., Kjeldsen H., 2009a, MNRAS, 400, 1945

Tabur V., Kiss L. L., Bedding T. R., 2009b, ApJ, 703, L72

Thé P. S., Thomas D., Christensen C. G., Westerlund B. E., 1990, PASP, 102, 565

Torrejón J. M., Negueruela I., Smith D. M., Harrison T. E., 2010, A&A, 510, A61

Tueller J. et al., 2010, ApJS, 186, 378
Turnshek D. E., Turnshek D. A., Craine E. R., Boeshaar P. C., 1985, An Atlas of Digital Spectra of Cool Stars. Western Research Co., Tucson
van Belle G. T. et al., 1999, AJ, 117, 521
Walter R., Zurita Heras J., 2007, A&A, 476, 335
Wilms J., Allen A., McCray R., 2000, ApJ, 542, 914
Yamauchi S. et al., 1995, PASJ, 47, 189
Zurita Heras J. A., Chaty S., 2009, A&A, 493, L1

This paper has been typeset from a TEX/LATEX file prepared by the author.